Evident structural anisotropies arising from near-zero particle asphericity in granular spherocylinder packings

Yuwen Sun,[1] Chenyang Wang,[1] Jing Yang,[1] Weijia Shi,[1] Qifan Pang,[1] Yujie Wang,[2,3,4] Jianqi Li,[1] Bingwen Hu,[1] and Chengjie Xia[1,*]

[1]*Shanghai Key Laboratory of Magnetic Resonance, School of Physics and Electronic Science, East China Normal University, Shanghai 200241, China*

[2]*School of Physics and Astronomy, Shanghai Jiao Tong University, Shanghai 200240, China*

[3]*State Key Laboratory of Geohazard Prevention and Geoenvironment Protection, Chengdu University of Technology, Chengdu 610059, China*

[4]*Department of Physics, College of Mathematics and Physics, Chengdu University of Technology, Chengdu 610059, China*

(Received 20 March 2024; accepted 2 July 2024; published 30 July 2024)

With magnetic resonance imaging experiments, we study packings of granular spherocylinders with merely 2% asphericity. Evident structural anisotropies across all length scales are identified. Most interestingly, the global nematic order decreases with increasing packing fraction, while the local contact anisotropy shows an opposing trend. We attribute this counterintuitive phenomenon to a competition between gravity-driven ordering aided by frictional contacts and a geometric frustration effect at the marginally jammed state. It is also surprising to notice that such slight particle asphericity can trigger non-negligible correlations between contact-level and mesoscale structures, manifested in drastically different nonaffine structural rearrangements upon compaction from that of granular spheres. These observations can help improve statistical mechanical models for the orientational order transformation of nonspherical granular particle packings, which involves complex interplays between particle shape, frictional contacts, and external force field.

DOI: 10.1103/PhysRevE.110.014903

I. INTRODUCTION

Particle packing models are important for studying molecular, colloidal, and granular assemblies, which can provide fundamental understandings for their complex macroscopic behaviors and transitions between their various phases [1]. It is well known that particle shape affects the packing structures, and correspondingly, mechanical and transport properties. Few quasiuniversal laws have been proposed for the shape effects of nonspherical packing systems based on expansion in the vicinity of the shape of a sphere [2,3]. Yet a hard sphere packing may not be a very reliable reference point for nonspherical particles even with very slight asphericity [4], since the packing structure and dynamics depend sensitively on particle shape [5–8]. A classic example is the sharp increase in packing fractions and average contact numbers of ellipsoid and spherocylinder packings when the particle shape changes slightly from a sphere [9–11]. Also, a sheared packing of spherocylinders exhibits nonzero nematic order in the limit of the particle shape approaching a sphere [12], and infinitesimal asphericity of ellipsoids leads to a distinct universality class of the jamming transition compared with spheres [13]. Thus it would be illuminating to examine how a random packing structure loses its assumed spherical symmetry when the particle shape begins to deviate from a sphere.

For granular matter, a member of the particle packing family, the particle shape effect is of fundamental and practical research interest as well [14]. Nonspherical granular packings sometimes show orientationally ordered phases and flow dynamics reminiscent of some liquid-crystalline systems [15,16], but their athermal nature can also lead to complex nonequilibrium behaviors, requiring fundamentally different theories. For example, for a granular packing, its statistical mechanical laws depend on the mechanical stability requirement which couples frictional contacts and particle orientations [17–19]. For a flowing granular system, additional interplays between particle orientations, contact forces, and anisotropic kinetics lead to convoluted dynamic behaviors [20–24]. Experimentally, the packing structures of some nonspherical granular particle packings have been studied with various imaging techniques [25,26]. Most previous studies have focused on particles with relatively large asphericity and other overwhelming shape effects, including the excluded volume effect of elongated particles [27], geometric cohesion effect of long rods [28], stack effect of thin plates [29], and flat contact effect of polyhedral particles [30,31], etc. Yet the mechanisms of some elementary particle shape effects remain elusive. For instance, a series of previous studies on nonspherical granular packings has discovered a counterintuitive diminishing of global orientational order upon compaction [29,32,33], while some others have reported an opposing trend [15,34]. These observations raise a most primary question: What is the fundamental law underlying the evolution of orientational order with packing fraction in a nonspherical granular packing? We think studying the packing structures of granular particles with very slight asphericity can provide some quasiuniversal understandings

*Contact author: cjxia@phy.ecnu.edu.cn

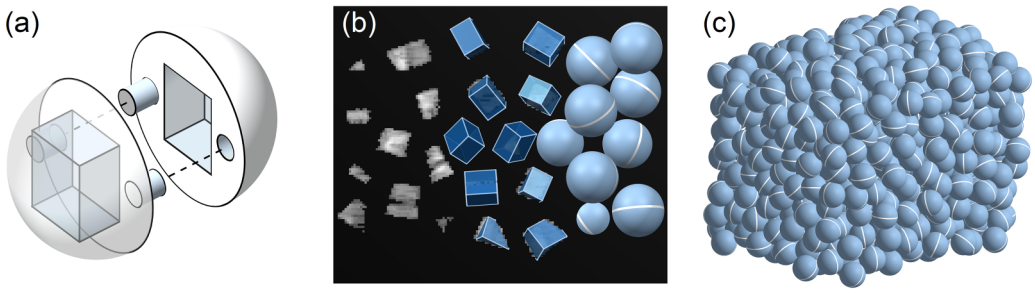

FIG. 1. (a) A schematic of assembling one spherocylinder with the two identical halves. When the two half spheres are attached, the short pillar on each part can be inserted into the opposing hole to fix their relative position and orientation, and the two cavities can merge into one hollow cuboid inside the particle. (b) One slice of the magnetic resonance image superimposed by reconstructed hydrogel-filled cuboids at the middle section of the graph, and spherocylinders at the right side. (c) A reconstructed spherocylinder packing. In (b), (c), the white belt on each particle indicates the cylindrical side wall and the particle orientation.

of the shape effects, and shed light on such unresolved problems.

In this work, we employ magnetic resonance imaging (MRI) techniques to reconstruct and study the packings of very short granular spherocylinders, whose aspect ratio, i.e., the ratio between the length and diameter of the spherocylinder, is only 1.02, in contrast with previous investigations on much longer spherocylinders [9,11,21,35,36]. Despite this extremely small particle asphericity, we are still able to observe evident structural anisotropies at different length scales. Interestingly, the global orientational order (i.e., nematic order) decreases with increasing packing fraction, while a local structural anisotropy associated with the contact orientations (i.e., the vectors connecting the particle centroid and contact points) increases. The opposing trends of anisotropies at global and contact levels indicate a general ordering transformation law of nonspherical granular particles, governed by a competition between gravity-driven ordering of individual particles stabilized by frictional contacts, and the marginal stability condition of a frictionless particle packing, (i.e., a critical packing state with just enough contacts to maintain mechanical stability [37]). The structural rearrangements at mesoscale have also been characterized, emphasized by a notably different scaling exponent from that of granular sphere packings owing to non-negligible coupling between particles' centroids and orientations induced by the slight asphericity. The geometric characterizations and structural transformation laws unveiled here can also provide insights into other out-of-equilibrium particle packing systems.

II. EXPERIMENTAL PROCEDURE AND DATA ANALYSIS METHOD

A. Spherocylinder particles

Each particle used in this experiment is composed of two identical plastic half spheres produced by 3D printing, as shown in Fig. 1(a). The diameter D of a half sphere is 23.48 ± 0.04 mm. When the two parts are glued together, there is a small gap of 0.54 ± 0.19 mm between them. The actual particle shape can be approximated as a spherocylinder with an aspect ratio of 1.02 with a thin groove replacing the cylindrical side. The absence of the cylindrical side in the particle's exterior shape barely affects the packing structures because we find no gathering of contact points near the groove, as would be assumed to happen when the particle shape nonconvexity is strong. Such a phenomenon has been observed in packings of granular spheres with holes whose nonconvexity is much larger than ours [38]. Furthermore, there is a $10 \times 12 \times 14$ mm^3 cuboid cavity at the center of each particle filled with hydrogel for magnetic resonance imaging. The densities of the particle shell and hydrogel are about 1.24 and 1.12 g/cm^3, respectively. For a homogeneous spherocylinder, the anisotropy index of the moment of inertia tensor is 0.98, measured as the ratio between the smallest and largest eigenvalues. The nonuniform mass distribution changes this anisotropy index by 1.8%, and also breaks the rotational symmetry around the spherocylinder axis with a 0.1% relative difference in the other two eigenvalues. The particle size polydispersity in D is about 0.16% and the standard deviation of the aspect ratio is about 8.3×10^{-3}. In this work, the average diameter of the spherocylinders is set as a unit length. The average surface friction coefficient between two particles is 0.33 ± 0.02, measured according to a sphere stacking method [39].

B. Shaking experiments

During the experiment, we first randomly poured the particles into a cuboid container with size $260 \times 200 \times 180$ mm^3. The internal wall and floor of the container are decorated with hemispheres with a diameter of 25 mm at random positions to reduce the ordering effect of flat boundaries. The loose initial packing state was scanned by an MRI scanner. Then the container was placed onto an electrical vibrator, and shaken vertically under a sinusoidal excitation with 30 Hz frequency and $2.6g$ peak acceleration (with g representing the gravitational acceleration). The packing fraction increased gradually under vibration, and the packing was scanned again after 1, 5, 10, and 100 s of shaking. These scanned packings correspond to different states during a compaction process, and we obtain packings with different packing fractions in this way. The packing fraction saturated after about 100 s of shaking, and this final packing state is close to the steady state under this vibration protocol. Four independently repeated compaction trials were carried out to increase the amount of data, and a total of nineteen packing structures are analyzed in this work.

C. MRI and image processing

The cavity of each particle is filled with hydrogel produced by edible gelatin, water, and glycerol to provide strong resonance signals, and thus it appears bright in the scanned image. The spatial resolution of the MRI scanner (MAGNETOM Prisma Fit, Siemens Healthcare, Erlangen, Germany) is 1mm/pixel. Through our image processing algorithm, the position and orientation of each cavity are calculated by optimizing the overlap between each region in the raw image and a model cuboid with the same size and shape [see Fig. 1(b)] and, accordingly, the whole packing structure is reconstructed [see Fig. 1(c)]. The optimizing process is similar to the one previously used to reconstruct packing structures of some other nonspherical granular particles [30]. We estimate the errors of centroid and particle orientation to be about $0.012D$ and 1.0°, respectively.

In the subsequent analyses, only particles at least $1D$ away from the container boundaries and the packing's upper surface are included, leaving about 350 particles in each packing. We have verified that the following results barely depend on the system size as long as more than 200 particles in each packing are included in the calculations.

D. Contact identification

Rigorous (mechanical) contacts are impossible to identify with imaging experiments, but we can identify (geometric) quasicontacts between particle pairs by setting a distance threshold δ_t for their interparticle distances δ. The interparticle distance between two particles is defined as the shortest distance between the two segments connecting the two spherocylinders' respective pairs of hemispherical centers minus D, and the contacts can be categorized into three forms: head-head, waist-waist, and head-waist [see Figs. 2(a)–2(c)]. The proper value of the threshold can be obtained with a well-developed approach. According to Aste *et al.* [40], interparticle distances between contact particles are assumed to follow a Gaussian distribution, considering the errors of reconstructed packing structures due to the finite resolution and gray scale fluctuations of the raw images. Also, the interparticle distances of nearby particles which are not in real contacts are assumed to follow a uniform distribution in a short distance range. Therefore, the average number of neighbors for all central particles whose interparticle distance is smaller than a threshold δ_t should have a form of an error function (i.e., erf) plus a linear function,

$$N(\delta_t) = \frac{Z}{2}\left[1 + \mathrm{erf}\left(\frac{\delta_t - \delta_{t,0}}{\Delta}\right)\right] + H(\delta_t - \delta_{t,0})K(\delta_t - \delta_{t,0}), \tag{1}$$

where H is the Heaviside step function; Z, $\delta_{t,0}$, Δ, and K are fitting parameters obtained by fitting the experimental data [see Fig. 2(d)]. Among these parameters, Z represents the actual average contact number, $\delta_{t,0}$ and Δ denote the average value and standard deviation of the interparticle distance between contact neighbors, and K represents the growth rate of noncontact neighbors with interparticle distance. The proper threshold δ_t^* is the one satisfying $N(\delta_t^*) = Z$, which equals $0.023D$ in this work.

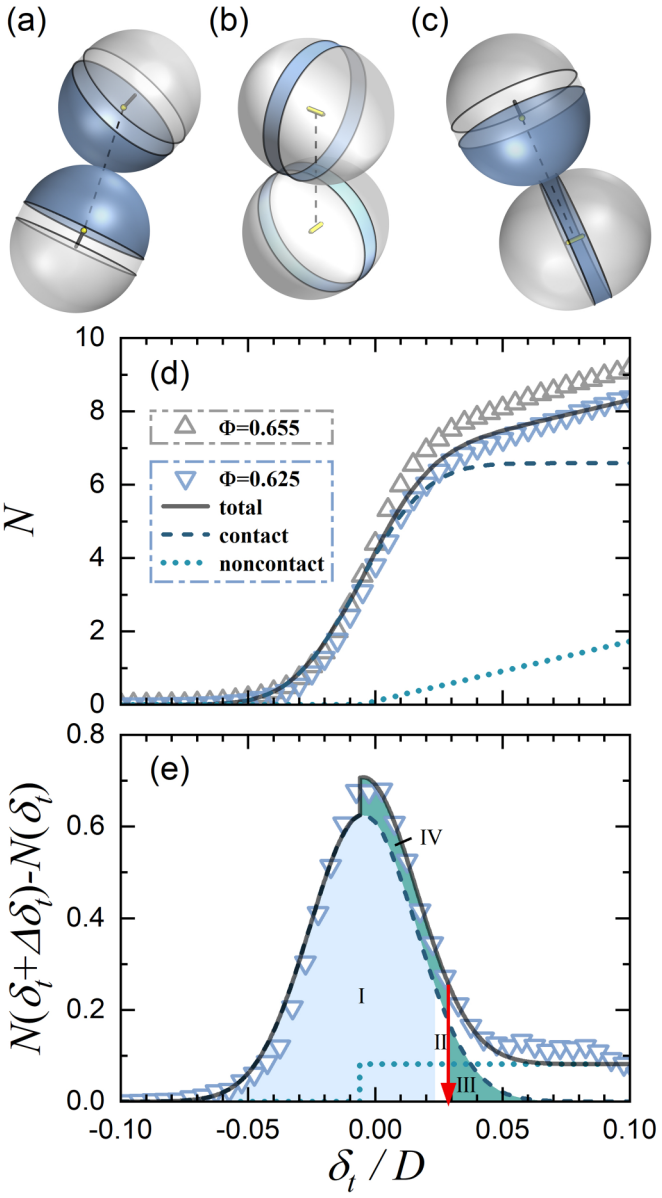

FIG. 2. Schematics of head-head (a), waist-waist (b), and head-waist (c) contact spherocylinders. The dashed line denotes the shortest distance between the segments connecting the two hemispherical centers of each particle. (d) Average number of nearby particles as a function of interparticle distance threshold δ_t, for two packings with $\Phi = 0.655$ (up triangles) and 0.625 (down triangles). The solid line is a fit of the $\Phi = 0.625$ experimental data, which is the sum of an error function (dashed line) and a linear function (dotted line). (e) Increment of average number of nearby particles when δ_t increases to $\delta_t + \Delta\delta_t$, where $\Delta\delta_t = 5 \times 10^{-3}D$. The lines are derivatives of the lines in (d) up to a multiplier $\Delta\delta_t$: the fitting curve (solid line) is the sum of a Gaussian function (dashed line) and a step function (dotted line). The red arrow marks the threshold δ_t^* that gives the correct average contact number of this packing. In this graph, the average contact number corresponds to the area under the Gaussian function, i.e., the summation of areas I, II, and III, which also equals the total area under the solid curve and to the left of the threshold, i.e., the summation of areas I, II and IV, up to the multiplier. The area of region I corresponds to $N = 6$, that is, the isostatic condition for spheres, and regions III and IV have equal areas by definition of the threshold.

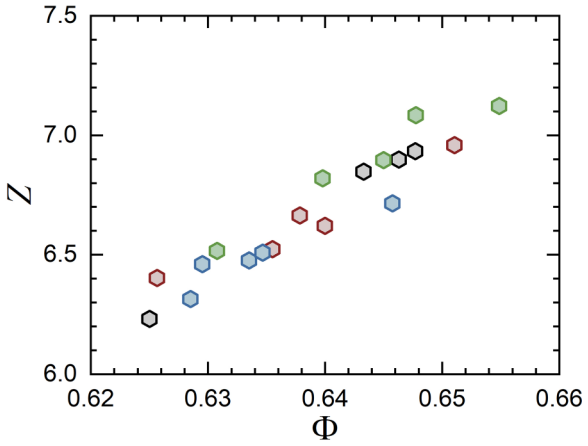

FIG. 3. Average contact numbers Z for packings with different packing fractions Φ. Data points with different colors correspond to packings of different compaction trials.

III. STRUCTURAL QUANTIFICATIONS

A. Contact number versus packing fraction

We first calculate some basic structural quantities of a granular packing. The packing fraction of a packing is defined as $\Phi = V_p/\langle V_{\text{cell}}\rangle$, where V_p is the average particle volume, and V_{cell} is the Voronoi cell volume of each particle calculated using a set-Voronoi method [41]. The average contact number Z of a packing is obtained using the above generalized error-function method. As shown in Figs. 2(e) and 3, the average contact numbers of all our packings are larger than that of the random close packing (RCP) state of granular spheres (i.e., 6), and the largest value is smaller than 10 (i.e., twice the number of degrees of freedom of a spherocylinder). This is consistent with the underconstrained jammed packing state of nonspherical particles [4]. Besides, by interpolating previous results of hard frictionless spherocylinders [11,42] and ellipsoids [8,10], we find that the packing state of our densest packing (i.e., $\Phi = 0.655$ and $Z = 7.12$) is close to the J points of these elongated frictionless particles with the same aspect ratio. Thus our densest packing is close to the RCP state because of the theoretical correspondence between the RCP of granular particles and the jamming transition critical point of frictionless particles [18,43].

B. Global nematic order

To determine whether gravity can introduce global orientational order in our system, we define a nematic order parameter $S = \langle P_2(\cos\theta)\rangle$, where P_2 is the second-order Legendre polynomial and θ is the angle between each spherocylinder's orientation and the vertical direction [see Fig. 4(a)]. According to this definition, $S = 0$ corresponds to an isotropic particle orientation distribution, while a negative S means that the particle orientations tend to point horizontally. As shown in Fig. 4(d), S of our loosest packing is negative and increases towards zero as packing fraction increases. To first determine whether such a small absolute value of S reflects true nematic order in the packing, or just results from the fluctuation of a small system, we generate 350 random orientations according to an isotropic orientation distribution, and calculate

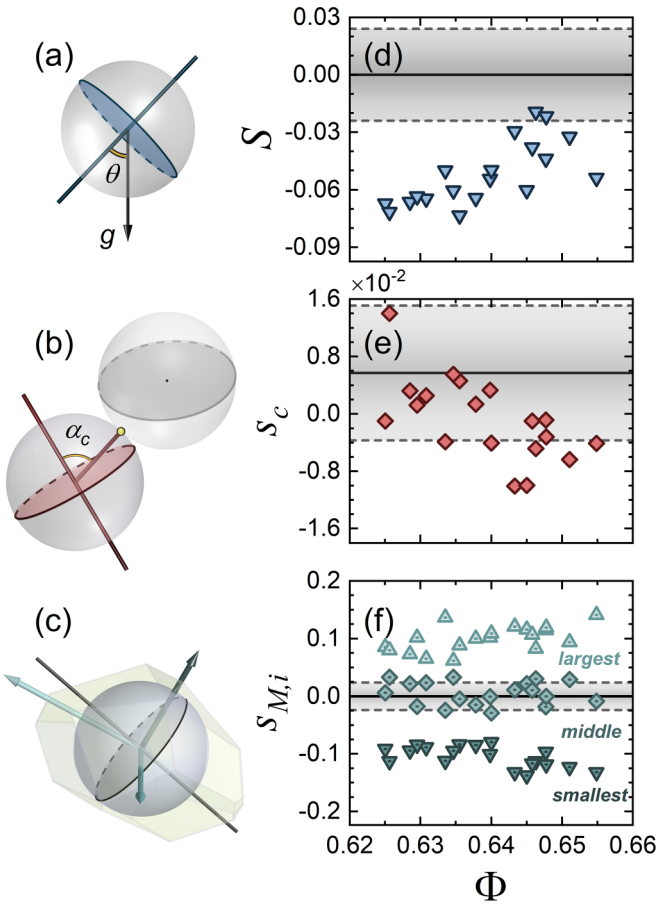

FIG. 4. Schematics for (a) the angle θ between particle orientation and gravitational direction for evaluating the nematic order parameter S, and (b) the angle between the central particle's orientation and a vector connecting its centroid and a contact point on its surface, to calculate the contact orientation order parameter s_c. (c) Voronoi cell of a particle. The angles between the particle orientation (black line) and the three eigenvectors (green arrows) of the cell are used to evaluate the cell orientation order parameter $s_{M,i}$. (d) The nematic order parameter S for packings with different packing fractions Φ. If the same number of particles follow an isotropic random orientation distribution, the expectation value of S is zero (solid line), and the standard deviation is 2.4×10^{-2} (dashed lines). (e) Contact orientation order parameter s_c for packings with different Φ. Assuming a uniform distribution of contacts on the particle surface, the expectation value of s_c is 0.57×10^{-2} (solid line), and its standard deviation is 0.94×10^{-2}, marked by half the width of the shaded region. (f) Cell orientation order parameters $s_{M,i}$ versus Φ, with i denoting eigenvectors corresponding to the largest ($i = 1$, up triangles), middle ($i = 2$, diamonds), and smallest ($i = 3$, down triangles) eigenvalues. The boundaries of the shaded region represent the standard deviation of these parameters if the particle and cell orientations were uncorrelated.

numerically the standard deviation $\sigma(S^{\text{iso}})$ of their fluctuating values of S, as marked by the shaded region in Fig. 4(d). $|S|$ being basically larger than $\sigma(S^{\text{iso}})$ leads to our conclusion that the nematic order truly exists. Similar comparisons between the actual data and completely random orientations have also been carried out in the following to confirm the existence of some ordering or correlation. Additionally, we have calculated the nematic order associated with the other two eigenvectors

of the moment of inertia tensor of the particle, which are perpendicular to the spherocylinder's orientation. Their nematic order is basically identical with each other, i.e., both equaling $-S/2$ within experimental error, indicating the negligible influence of the anisotropic moment of inertia tensor.

It is counterintuitive that the global orientational order gradually decreases upon compaction, which appears to be the very opposite of the entropy-driven excluded volume effect of elongated hard particles. Therefore, the emergence of the global orientational order in our granular spherocylinder packings should be majorly mechanical. We have also verified that the same nematic order parameter is always negligible if it is calculated along horizontal directions, proving its gravitational origin, but why the anisotropic influence of gravity on a looser packing is more noticeable can only be answered after the following analyses are made on packing structures at a much smaller length scale.

C. Contact orientation order parameter

The contact-level structures are crucial to understanding the mechanical stability properties of a granular packing. The mystery that a jammed packing of frictionless nonspherical particles is mechanically stable but has fewer contacts than the isostatic condition has been partly solved by considering the vibrational modes with zero or quartic energy terms near the jamming transition [4,6,44,45]. According to previous studies, contacts near the waist of an elongated particle can provide more constraints to the degree of freedom, since they can block translational and rotational movements at the same time, and thus form a hypostatic jammed packing [2,4,5]. It is unclear whether this mechanism is responsible for the orientational order transformation in random packings of frictional nonspherical particles. Thus we characterize the anisotropy of contact structures with a contact orientation order parameter, and an orientational distribution of contact points on each central particle. Interestingly, the evolving trend of the local structural anisotropy associated with the contact structures is opposite to S, as elaborated upon below.

We first define a contact orientation unit vector $\mathbf{n}_c$ along the direction from the particle centroid to a contact point. The contact angle α_c is the (acute) angle between $\mathbf{n}_c$ and the central particle's orientation [see Fig. 4(b)]. We define a contact orientation order parameter $s_c = \langle P_2(\cos\alpha_c)\rangle$ to characterize the contact anisotropy, where the average is calculated over all pairs of contacts. It would equal $s_c^{\rm uni} = 0.57 \times 10^{-2}$ if all contact points were distributed uniformly on the particle surface (i.e., with an equal number of contacts per unit area). This value is nonzero because of the particle asphericity, and we compare s_c with this reference value to tell how differently the contacts are distributed on the particle surface from a uniform distribution. As demonstrated in Fig. 4(e), s_c are basically smaller than $s_c^{\rm uni}$, indicating a slight preference of contact points to be located close to the spherocylinder's waist. Also, the progressively smaller value of s_c with respect to $s_c^{\rm uni}$ when Φ increases is in contrast to S, indicating competing rearranging mechanisms at local and global levels.

To understand the origin of the increasing contact-level anisotropy with Φ more comprehensively, we calculate the probability distribution function (PDF) $f(\alpha_c)$ of α_c. As shown in Fig. 5(a), when $f(\alpha_c)$ is normalized by $f^{\rm uni}(\alpha_c)$, which is the contact angle PDF assumed for uniformly distributed contact points on the particle surface, two unusual peaks at roughly 40° and 80° irrespective of Φ can be distinguished. The two peaks are relatively higher for denser packings. Inspired by a previous theoretical result [46], we think the two peaks most likely originate from the symmetry of an icosahedron. According to Schaller *et al.* [46], for ellipsoids with near-zero asphericity, the densest local configuration adopts the structure of an icosahedral cluster approximately, and the orientation of the central ellipsoid is parallel with one face normal vector of the icosahedron. In such a configuration, the contact angles between neighboring and central ellipsoids are around 37° or 79° [as illustrated in Fig. 5(b)]. Therefore, the two peaks near the two characteristic angles demonstrate a noticeable residual influence of the densest local configuration in granular packings. This influence is preserved even in the loose packings which hardly contain any local

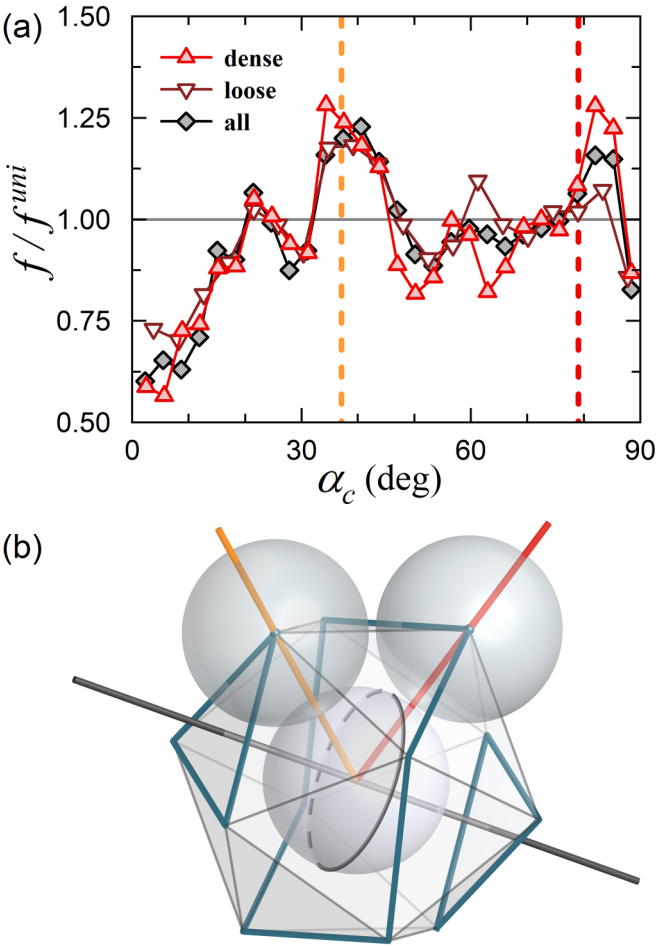

FIG. 5. (a) Averaged PDFs of α_c for the densest (up triangles) and loosest (down triangles) three packings, and for all packings (diamonds), all normalized by the PDF assuming a uniform contact point distribution. The two dashed lines mark 37° and 79°, corresponding to the included angles between a normal vector of a regular icosahedron's face and vectors connecting the icosahedron's center and vertices, as shown by the yellow and red lines in (b). (b) A schematic of an icosahedral cluster, with one particle at its center and neighbors at its vertices.

structures close to an intact icosahedral cluster. In addition, in this densest local configuration, the waists of the neighboring particles are directed at the central one, consistent with the smaller values of s_c than $s_c^{\rm uni}$, especially when Φ is large [see Fig. 4(e)]. Apparently such dense local structures are incommensurate with the global nematic order.

Based on the above structural analyses, the following mechanism for the orientational order transformation of nonspherical granular packings can be proposed, highlighting a complex interplay between friction and packing effects [47]. A dense granular packing is close to a marginally jammed packing of frictionless hard particles [18,43], requiring just enough contacts to constraint all collective modes [37]. Accordingly, for a spherocylinder packing, locally favored structures with more contacts near the particle waist increase with packing fraction and, hence, diminish the global nematic order analogously to a geometric frustration effect. In comparison, the frictional forces are more activated in a looser packing [48], which helps stabilize the structure with fewer contacts per particle regardless of the relative orientations and contact positions of the contact neighbors [49]. Therefore, each individual particle is allowed to take an orientation closer to the horizontal to lower its gravitational potential energy. In other words, the anisotropic influence of gravity on a looser packing appears to be more noticeable. This phenomenon is analogous to a transformation between a high-temperature paramagnetic phase and a low-temperature antiferromagnetic phase.

Besides, in previous numerical results of two-dimensional (2D) frictionless spherocylinder packings [12,50,51], exceedingly more contacts are detected to be exactly at the particle waist, i.e., at $\alpha_c \approx 90^\circ$, in the limit of zero asphericity. This is in stark contrast with the $f(\alpha_c)$ obtained in our frictional granular packings, although the underlying mechanisms of these different systems being hypostatic may have some connections. Moreover, in 2D sheared frictionless spherocylinder packings [52,53], similar evolutions of the nematic order and contact orientation order with packing fraction have been observed in the regime below jamming. Since a granular packing can be mapped onto a supercooled hard particle liquid at different temperatures or packing fractions [54], we believe that the mechanism of competing mechanical and geometric effects in dense nonspherical particle packings applies to both systems.

D. Voronoi cell anisotropy

The above results also remind us of the correlation between the anisotropic Voronoi cells and locally favored structures observed in granular sphere packings [55], indicating a discernible correlation between the central particle's orientation and the packing structures at a slightly larger length scale than the contact level. Thus we proceed to analyze the Voronoi cell structure to quantify this correlation. The shape anisotropy of a Voronoi cell can be quantified by a Minkowski tensor, $\boldsymbol{M} = \int \mathbf{r} \otimes \mathbf{r} dV$, where $\mathbf{r}$ is a vector from the cell's geometric center to each point in the cell, and the integral is calculated over the cell volume [56]. The eigenvector of $\boldsymbol{M}$ associated with the largest (smallest) eigenvalue corresponds to the direction where the cell is most elongated (shortened) [Fig. 4(c)]. We define a triplet of parameters $s_{M,i} = \langle P_2(\cos\gamma_i)\rangle$ to characterize the eigenvectors' direction with respect to the spherocylinder's orientation, where γ_i is the (acute) angle between each particle's orientation and the ith eigenvector of $\boldsymbol{M}$, with $i = 1,\ 2,\ 3$ representing the one associated with the largest, middle, and smallest eigenvalues, respectively. The average is calculated over all particles. As shown in Fig. 4(f), $s_{M,1}$ ($s_{M,3}$) is positive (negative) for all packing fractions, clearly manifesting a tendency of the spherocylinders to align with the cell elongation direction [57]. Since the Voronoi cells are anisotropic even in a random packing of spheres [56], the clear correlation between particle orientation and a cell's eigenvector observed here is not only trivially due to the elongated particle shape, but also the mild tendency of a central spherocylinder to have more contact neighbors near its waist, leaving relatively large voids along the particle orientation. Consistently, the absolute values of $s_{M,1}$ and $s_{M,3}$ increase slightly with Φ similar to $|s_c - s_c^{\rm uni}|$, indicating an extension of the above inherent packing effect on the contact structures to the Voronoi structures in jammed packings. This may also cause anisotropic and correlated dynamics of the particles when the packing is perturbed [58].

E. Nonaffine evolution of local and mesoscale structures

A final piece of the puzzle is how to bridge the opposing trends of the structural anisotropies at global and contact levels. To this end, we analyze the particle shape effects across different length scales in the following systematic way. For each central particle, we sort all nearby particles by their centroid-centroid distances $r_{ij} = |\boldsymbol{r}_{ij}|$, where $\boldsymbol{r}_{ij}$ is a vector connecting the particle centroids. Then we calculate $\langle r_{ij}\rangle_k$, where $\langle\cdots\rangle_k$ represents an average among all central particles and their respective nearest k neighbors. Power-law relationships $\Phi \propto \langle r_{ij}\rangle_k^{-d_k}$ are observed for all values of k with a varying exponent d_k [Fig. 6(a)]. This exponent should equal the spatial dimension regardless of k from a simple dimensional analysis, but this trivial scaling law only holds for particle systems with negligible spatial correlation such as a simple liquid, and ordered point arrays like a crystal, while discrepancies of a similar exponent from the spatial dimension have been observed in amorphous solids [59]. This conundrum has been attributed to the nonaffine structural rearrangements within the local packing structures when the packing fraction changes [60]. The extent of structural transformation nonaffinity can be measured by the difference of the scaling exponent from the spatial dimension. It is most intriguing that this exponent has a minimal value $d_k \approx 2.1$ at $k = 12$ [see Fig. 6(b)], in comparison with the minimal value $d_{13} \approx 2.5$ for granular sphere packings [60], which means that the merely 2% shape change from a sphere to a spherocylinder causes a substantially 18% change of the exponent. The smaller exponent for granular spherocylinder packings implies a more sensitive response of the centroid-centroid distance when the packing fraction changes compared with the granular sphere packings. This additional "softness" clearly originates from the accompanied evolution of nearby particles' relative orientations when the packing fraction changes, indicating a remarkable correlation between the orientational and translational degrees of freedom.

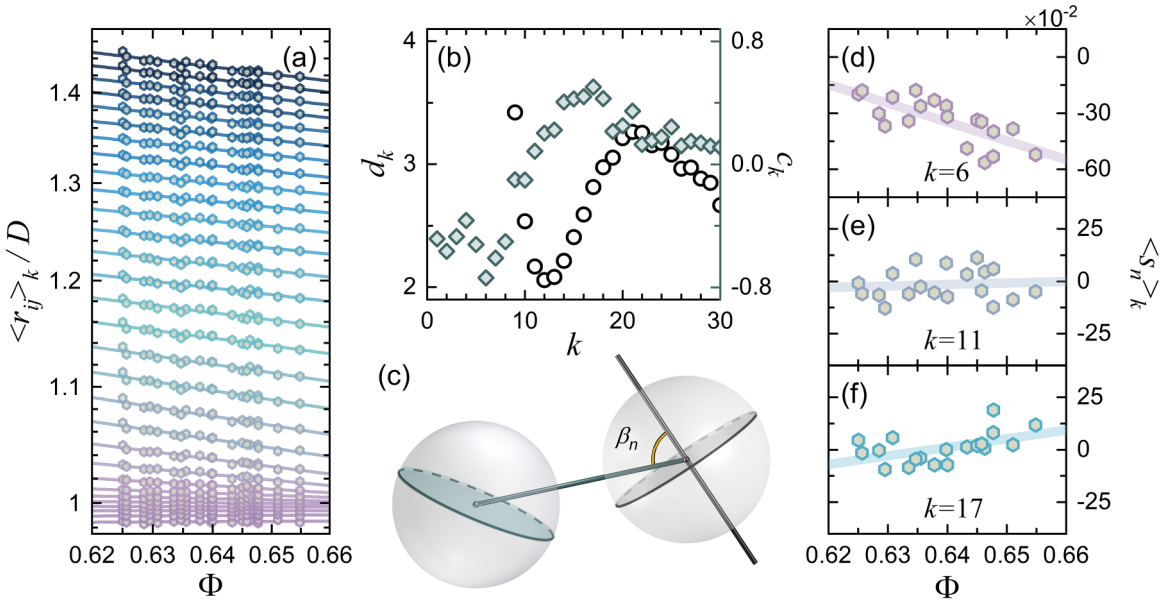

FIG. 6. (a) The average centroid-centroid distances between the central particle and its nearest k neighbors for packings with different Φ. The lines are power-law fittings of the experimental data: $\langle r_{ij}\rangle_k \propto \Phi^{-1/d_k}$. The data from bottom to top correspond to k ranging from 1 to 30. (b) The fitted exponent d_k (circles, left axis) and the correlation coefficient c_k between $\langle s_n\rangle_k$ and Φ (diamonds, right axis) for different k. (c) A schematic of the angle β_n between the orientation of a nearby particle and a vector connecting the centroids of it and the central particle, for evaluating the neighbor orientation order parameter s_n. Average neighbor orientation order parameter $\langle s_n\rangle_k$ for packings with different Φ, for $k = 6$ (d), 11 (e), and 17 (f). The solid lines are linear fittings of the data.

To further quantify the statistic changes of relative orientations of granular spherocylinders, we develop a neighbor orientation order parameter $s_n = P_2(\cos\beta_n)$, with β_n denoting the (acute) angle between $\boldsymbol{r}_{ij}$ and the orientation of each nearby particle [see Fig. 6(c)]. We obtain different relationships between $\langle s_n\rangle_k$ and Φ for different k, as shown in Figs. 6(d)–6(f). In general, the correlation coefficients c_k between $\langle s_n\rangle_k$ and Φ are negative for $k < 11$, suggesting that, for particles within the first shell of a central particle, directing their waists towards the central particle makes comparatively dense packing structures. In comparison, c_k are positive for $k \geqslant 11$, which means that facing the central particle with their heads may efficiently accommodate more particles in the second shell and increase the packing fraction. c_k approaches zero for large enough k, representing a dying-out long-range spatial correlation. Hence, the packing effect has conflicting influences on the relative orientations of particles within the first shell and those beyond, but the dense structures at both levels prefer particles to misalign with each other, further decreasing the global nematic order upon compaction. We also suspect that the mesoscale nonaffine structural rearrangements associated with both translational and rotational movements are deeply connected with the phonon modes of nonspherical particles [61].

IV. DISCUSSION AND CONCLUSION

In this work, we report structural anisotropies in granular spherocylinder packings. The existence of global nematic order due to gravity is expected. Nonetheless, the structural anisotropies triggered by the very slight 2% particle asphericity at both contact-level and Voronoi structures are rather unexpected and nontrivial. The physical mechanism of the orientational order transformation of nonspherical granular materials is now clear. For a loose packing away from the RCP state, the orientational order is influenced by lowering the gravitational potential of individual particles, with frictional contacts at random positions helping stabilize the configurations. For a dense packing, as it approaches the marginally stable jammed state of frictionless particles, the global orientational order is determined by the orientational symmetry of the locally favored dense structures, for example, whether they are commensurate with a nematic phase.

This mechanism should be general, at least in a moderate range of particle asphericity, since it originates from the fundamental marginal stability of jammed materials, and it potentially connects the structural transformation laws of granular materials with the theoretical advance of the glass and jamming transitions of nonspherical particles [13]. For particles with stronger particle asphericity, e.g., more elongated granular spherocylinders or rods, the larger variation range of the nematic order parameter observed in previous studies is a natural corollary based on the above mechanism [15,62]. Our previous explanation of a similar decreasing (increasing) global (local) orientational order of granular disks upon compaction can also be incorporated into this theoretical scenario [29]. Moreover, for particles with different surface friction properties, one can anticipate a weakened nematic order for a less frictional nonspherical granular packing. Consistently, we have observed an orientationally random RCP state of almost frictionless hydrogel ellipsoids [63]. Systematic studies to fully clarify the individual roles played by particle shape and friction should be carried out in the future.

Furthermore, the findings of the present work clearly demonstrate nonignorable couplings between the particle's orientational and translational degrees of freedom, and

between contact-level and Voronoi structures of nonspherical granular packings, which are very weak in granular sphere packings [54,64]. These analyses therefore pose a demanding challenge to the statistical mechanical models of granular packings based on the Edwards volume and/or stress ensembles [65,66], since most current models are based on simplified mean-field assumptions. In principle, one should take into consideration the intricate interplays between particle shape, frictional contacts, and external force field to model correctly the ubiquitous packing structural transformation accompanied with orientational order evolution. Notice that all the above subtle correlations can emerge vividly even when particle asphericity is as small as 2%.

To go one step further, the situation can be more complex if kinetic effects are taken into consideration. For a granular system under mechanical agitation, the kinetic energy tends to dilate the packing and destroy global orientational order due to entropic reasons, while on the contrary, the higher configurational temperature (i.e., the effective granular temperature in the Edwards volume ensemble [19]) for a looser packing implies a stronger influence of the external force that aligns particle orientations. The competing effects of kinetic and configurational temperatures could be a statistical mechanical origin of the complex constitutive relations of slowly agitated dense granular flows [20–22]. A careful examination of the structural anisotropies at various length scales as done here could be crucial to understanding them.

ACKNOWLEDGMENTS

The authors thank Jie Zhang and Chunmei Wang for helping prepare the samples. This work is supported by the National Natural Science Foundation of China (Grants No. 11904102 and No. 12274292) and the East China Normal University Outstanding Academic Training Program for Future Leading Talents (Grant No. 2024ZY-004).

[1] S. Torquato, J. Chem. Phys. **149**, 020901 (2018).
[2] J. X. Tian, Y. P. X. Xu, Y. Jiao, and S. Torquato, Sci. Rep. **5**, 16722 (2015).
[3] Y. Kallus, Soft Matter **12**, 4123 (2016).
[4] A. Donev, R. Connelly, F. H. Stillinger, and S. Torquato, Phys. Rev. E **75**, 051304 (2007).
[5] Y. Jiao, F. H. Stillinger, and S. Torquato, Phys. Rev. E **81**, 041304 (2010).
[6] C. F. Schreck, N. Xu, and C. S. O'Hern, Soft Matter **6**, 2960 (2010).
[7] S. W. Zhao, N. Zhang, X. W. Zhou, and L. Zhang, Powder Technol. **310**, 175 (2017).
[8] Y. Yuan, K. VanderWerf, M. D. Shattuck, and C. S. O'Hern, Soft Matter **15**, 9751 (2019).
[9] S. R. Williams and A. P. Philipse, Phys. Rev. E **67**, 051301 (2003).
[10] A. Donev, I. Cisse, D. Sachs, E. A. Variano, F. H. Stillinger, R. Connelly, S. Torquato, and P. M. Chaikin, Science **303**, 990 (2004).
[11] J. Zhao, S. X. Li, R. P. Zou, and A. B. Yu, Soft Matter **8**, 1003 (2012).
[12] T. Marschall, Y. E. Keta, P. Olsson, and S. Teitel, Phys. Rev. Lett. **122**, 188002 (2019).
[13] C. Brito, H. Ikeda, P. Urbani, M. Wyart, and F. Zamponi, Proc. Natl. Acad. Sci. USA **115**, 11736 (2018).
[14] T. Borzsonyi and R. Stannarius, Soft Matter **9**, 7401 (2013).
[15] F. X. Villarruel, B. E. Lauderdale, D. M. Mueth, and H. M. Jaeger, Phys. Rev. E **61**, 6914 (2000).
[16] T. Borzsonyi, B. Szabo, G. Toros, S. Wegner, J. Torok, E. Somfai, T. Bien, and R. Stannarius, Phys. Rev. Lett. **108**, 228302 (2012).
[17] C. C. Mounfield and S. F. Edwards, Phys. A **210**, 279 (1994).
[18] A. Baule, F. Morone, H. J. Herrmann, and H. A. Makse, Rev. Mod. Phys. **90**, 015006 (2018).
[19] S. F. Edwards and R. B. S. Oakeshott, Phys. A **157**, 1080 (1989).
[20] M. Trulsson, J. Fluid Mech. **849**, 718 (2018).
[21] T. Nath and C. Heussinger, Euro. Phys. J. E **42**, 157 (2019).
[22] D. B. Nagy, P. Claudin, T. Borzsonyi, and E. Somfai, New J. Phys. **22**, 073008 (2020).
[23] K. A. Murphy, A. K. MacKeith, L. K. Roth, and H. M. Jaeger, Granular Matter **21**, 72 (2019).
[24] Y. X. Zou, G. Ma, S. W. Zhao, S. S. Chen, and W. Zhou, Powder Technol. **416**, 118235 (2023).
[25] A. Amon, P. Born, K. E. Daniels, J. A. Dijksman, K. Huang, D. Parker, M. Schroeter, R. Stannarius, and A. Wierschem, Rev. Sci. Instrum. **88**, 051701 (2017).
[26] R. Stannarius, Rev. Sci. Instrum. **88**, 051806 (2017).
[27] A. P. Philipse, Langmuir **12**, 1127 (1996).
[28] Y. Bhosale, N. Weiner, A. Butler, S. H. Kim, M. Gazzola, and H. King, Phys. Rev. Lett. **128**, 198003 (2022).
[29] Y. Ding, J. Yang, C. Wang, Z. Wang, J. Li, B. Hu, and C. Xia, Phys. Rev. Lett. **131**, 098202 (2023).
[30] M. Neudecker, S. Ulrich, S. Herminghaus, and M. Schröter, Phys. Rev. Lett. **111**, 028001 (2013).
[31] Y. H. Ding, J. Yang, Y. Ou, Y. Zhao, J. Q. Li, B. W. Hu, and C. J. Xia, J. Phys.: Condens. Matter **34**, 224003 (2022).
[32] J. Q. Gan and A. B. Yu, Powder Technol. **361**, 424 (2020).
[33] F. M. Schaller, M. Neudecker, M. Saadatfar, G. W. Delaney, G. E. Schröder-Turk, and M. Schröter, Phys. Rev. Lett. **114**, 158001 (2015).
[34] Y. Ding, D. Gong, J. Yang, Z. Xu, Z. Wang, J. Li, B. Hu, and C. Xia, Soft Matter **18**, 726 (2022).
[35] L. Y. Meng, Y. Jiao, and S. X. Li, Powder Technol. **292**, 176 (2016).
[36] C. Heussinger, Phys. Rev. E **102**, 022903 (2020).
[37] A. J. Liu and S. R. Nagel, Annu. Rev. Condens. Matter Phys. **1**, 347 (2010).
[38] A. Peshkov, M. Girvan, D. C. Richardson, and W. Losert, Phys. Rev. E **100**, 042905 (2019).
[39] R. Cross, Phys. Educ. **55**, 055013 (2020).
[40] T. Aste, M. Saadatfar, and T. J. Senden, Phys. Rev. E **71**, 061302 (2005).
[41] F. M. Schaller, S. C. Kapfer, M. E. Evans, M. J. F. Hoffmann, T. Aste, M. Saadatfar, K. Mecke, G. W. Delaney, and G. E. Schroder-Turk, Philos. Mag. **93**, 3993 (2013).

[42] H. I. González and G. Cinacchi, J. Phys. Chem. B **127**, 6814 (2023).
[43] G. Parisi and F. Zamponi, Rev. Mod. Phys. **82**, 789 (2010).
[44] M. Mailman, C. F. Schreck, C. S. O'Hern, and B. Chakraborty, Phys. Rev. Lett. **102**, 255501 (2009).
[45] K. Shiraishi, H. Mizuno, and A. Ikeda, J. Phys. Soc. Jpn. **89**, 074603 (2020).
[46] F. M. Schaller, R. F. B. Weigel, and S. C. Kapfer, Phys. Rev. X **6**, 041032 (2016).
[47] Y. Yuan, Y. Jiao, Y. J. Wang, and S. X. Li, Phys. Rev. Res. **3**, 033084 (2021).
[48] S. Papanikolaou, C. S. O'Hern, and M. D. Shattuck, Phys. Rev. Lett. **110**, 198002 (2013).
[49] G. W. Delaney, J. E. Hilton, and P. W. Cleary, Phys. Rev. E **83**, 051305 (2011).
[50] T. Marschall and S. Teitel, Phys. Rev. E **97**, 012905 (2018).
[51] K. VanderWerf, W. Jin, M. D. Shattuck, and C. S. O'Hern, Phys. Rev. E **97**, 012909 (2018).
[52] T. A. Marschall and S. Teitel, Phys. Rev. E **100**, 032906 (2019).
[53] T. A. Marschall, D. Van Hoesen, and S. Teitel, Phys. Rev. E **101**, 032901 (2020).
[54] Y. Xing, Y. Yuan, H. F. Yuan, S. Y. Zhang, Z. K. Zeng, X. Zheng, C. J. Xia, and Y. J. Wang, Nat. Phys. **20**, 646 (2024).
[55] C. J. Xia, Y. X. Cao, B. Q. Kou, J. D. Li, Y. J. Wang, X. H. Xiao, and K. Fezzaa, Phys. Rev. E **90**, 062201 (2014).
[56] G. E. Schroder-Turk, W. Mickel, M. Schroter, G. W. Delaney, M. Saadatfar, T. J. Senden, K. Mecke, and T. Aste, Europhys. Lett. **90**, 34001 (2010).
[57] F. M. Schaller *et al.*, Europhys. Lett. **111**, 24002 (2015).
[58] S. Slotterback, M. Toiya, L. Goff, J. F. Douglas, and W. Losert, Phys. Rev. Lett. **101**, 258001 (2008).
[59] D. Z. Chen, Q. An, W. A. Goddard, and J. R. Greer, Phys. Rev. B **95**, 024103 (2017).
[60] C. J. Xia *et al.*, Phys. Rev. Lett. **118**, 238002 (2017).
[61] P. J. Yunker, K. Chen, Z. X. Zhang, W. G. Ellenbroek, A. J. Liu, and A. G. Yodh, Phys. Rev. E **83**, 011403 (2011).
[62] Y. Fu, Y. Xi, Y. X. Cao, and Y. J. Wang, Phys. Rev. E **85**, 051311 (2012).
[63] Y. F. Chen, M. Yuan, Z. C. Wang, Y. Zhao, J. Q. Li, B. W. Hu, and C. J. Xia, Soft Matter **17**, 2963 (2021).
[64] H. A. Vinutha and S. Sastry, Nat. Phys. **12**, 578 (2016).
[65] C. Song, P. Wang, and H. A. Makse, Nature (London) **453**, 629 (2008).
[66] A. Baule, R. Mari, L. Bo, L. Portal, and H. A. Makse, Nat. Commun. **4**, 2194 (2013).